Human Molecular Genetics, 2010, Vol. 19, No. 9 ***1741–1755***
doi:10.1093/hmg/ddq050
Advance Access published on February 10, 2010

Transgenic mice expressing mutant forms VCP/p97 recapitulate the full spectrum of IBMPFD including degeneration in muscle, brain and bone

Sara K. Custer[1], Manuela Neumann[2], Hongbo Lu[3], Alexander C. Wright[4] and J. Paul Taylor[1,*]

[1]Department of Developmental Neurobiology, St. Jude Children's Research, Hospital, Memphis, TN 38105, USA, [2]Institute of Neuropathology, University Hospital of Zurich, Zurich, Switzerland, [3]Gene Therapy Program, Department of Pathology and Laboratory Medicine, University of Pennsylvania School of Medicine, Philadelphia, PA 19104, USA and [4]Department of Radiology, University of Pennsylvania School of Medicine, Philadelphia, PA 19104, USA

Received December 7, 2009; Revised and Accepted February 3, 2010

Inclusion body myopathy associated with Paget's disease of bone and frontotemporal dementia (IBMPFD) is a dominantly inherited degenerative disorder caused by mutations in the valosin-containing protein (VCP) gene. VCP (p97 in mouse, TER94 in *Drosophila melanogaster* and CDC48 in *Saccharomyces cerevisiae*) is a highly conserved AAA$^+$-ATPase that regulates a wide array of cellular processes. The mechanism of IBMPFD pathogenesis is unknown. Towards elucidating the pathogenic mechanism we have developed and characterized transgenic mice with ubiquitous expression of wild-type and disease-causing versions of human VCP/p97. Here, we report that mice expressing VCP/p97 harboring the mutations R155H or A232E develop pathology that is limited to muscle, brain and bone, recapitulating the spectrum of disease in humans with IBMPFD. The mice exhibit progressive muscle weakness and pathological examination of muscle shows classic characteristics of inclusion body myopathy including rimmed vacuoles and TDP-43 pathology. The mice exhibit abnormalities in behavioral testing and pathological examination of the brain shows widespread TDP-43 pathology. Furthermore, radiological examination of the skeleton reveals that mutant mice develop severe osteopenia accompanied by focal lytic and sclerotic lesions in vertebrae and femur. *In vitro* studies indicate that mutant VCP causes inappropriate activation of the NF-κB signaling cascade, which could contribute to the mechanism of pathogenesis in multiple tissues including muscle, bone and brain.

INTRODUCTION

Inclusion body myopathy with Paget's disease of bone and frontotemporal dementia (IBMPFD) is a rare, autosomal dominant disorder characterized by the presence of at least three distinct disease pathologies of variable penetrance within a given kindred (1). Each of these disease pathologies—inclusion body myopathy (IBM), Paget's disease of bone (PDB) and frontotemporal dementia (FTD)—also exists individually as a common sporadic disorder. Muscle weakness with mild to severe myopathy is the most common clinical feature in IBMPFD, present in 80–90% of affected individuals. Radiographic and biochemical abnormalities consistent with PDB are observed in 43–51% of IBMPFD patients, although the age of onset (~42 years) is earlier than its sporadic counterpart. The dementia in IBMPFD is typical of FTD-TDP and is characterized by language and behavioral abnormalities, and typically presents later than both the IBM and PDB with a mean age of onset of 54 years (2).

IBMPFD is caused by mutations in the gene valosin-containing protein (VCP/p97) (3). Arginine 155 is the most common amino acid affected, with mutations at this position occurring in more than 50% of IBMPFD families. Substitution of this arginine residue to histidine (R155H) is the most common VCP mutation linked to IBMPFD. Mutation of alanine 232 to glutamic acid (A232E) is associated with a more severe clinical presentation, characterized by earlier onset of paget's disease of bone and a particularly aggressive myopathy. To date, a total of 14 VCP gene mutations have been reported in more than twenty families (3–8).

*To whom correspondence should be addressed at: Developmental Neurobiology, MS 343, D-4026, St. Jude Children's Research Hospital, 262 Danny Thomas Place, Memphis, TN 38105-3678, USA. Tel: +1 9015956047; Fax: +1 9015952032; Email: jpaul.taylor@stjude.org

VCP is a type II AAA^+ protein (*A*TPase *A*ssociated with diverse cellular *A*ctivities). VCP activity is essential for multiple aspects of ubiquitin-dependent signaling, including proteasome-mediated degradation of regulatory proteins such as IκB-α. Knockout of murine VCP/p97 results in early embryonic lethality, underscoring the importance of this gene's activity (9). The diversity in VCP/p97 activities reflects its ability to interact with a diverse array of adaptor proteins via N-terminal adaptor-binding domain. Most disease-causing mutations in VCP span the interface of the N-terminal domain and the D1 ATPase domain, leading to speculation about interference with a subset of adaptor-dependent interactions, although this as yet to be substantiated by evidence (10). The dominant mode of inheritance in IBMPFD suggests a toxic gain of function and this notion is supported evidence that disease-causing VCP mutations actually increase ATPase activity relative to wild-type, although a dominant negative mechanism cannot be excluded (11). The precise mechanism whereby mutations in VCP result in IBMPFD is unknown, and the basis for the selective vulnerability of brain, muscle and bone remains elusive although recent reports indicate that disease mutations in VCP compromise autophagy (12,13).

IBMPFD pathology is characterized by nuclear and cytoplasmic inclusions that are ubiquitin-positive but VCP-negative (14). These inclusions are immunopositive for the protein TAR DNA-binding protein 43 (TDP-43), a feature that links this pathology to a broad array of sporadic and inherited diseases including frontotemporal lobar degeneration with TDP-43 pathology (FTLD-TDP) and amyotrophic lateral sclerosis (ALS) (15). In these diseases, TDP-43 redistributes from the nucleus to the cytoplasm, and this change in subcellular localization correlates with cellular toxicity.

Aspects of the muscle pathology in IBMPFD have been previously modeled by transgenic expression of VCP with the R155H mutation under control of the muscle creatine kinase promoter (16). However, there remains a need for an animal model that captures the full spectrum of pathologies seen in IBMPFD, including involvement of muscle, brain and bone. Here, we demonstrate that transgenic mice with ubiquitous transgenic expression of mutant VCP recapitulate all aspects of IBMPFD including IBM with TDP-43 pathology, cognitive abnormalities accompanied by widespread TDP-43 pathology in brain, and bone abnormalities with similarities to PDB. Despite widespread expression in other tissues—including heart, liver, kidney, spleen and gut—this is not associated with pathology. In addition, we show that mutant VCP accelerates the turnover of IκB-α, leading to inappropriate activation of the NF-κB signaling cascade, which could contribute to the mechanism of pathogenesis in multiple tissues including muscle, bone and brain.

RESULTS

Generation and characterization of transgenic mice

To generate mice expressing VCP in all tissues, human VCP cDNA was expressed under the control of the CMV-enhanced chicken beta-actin promoter. This promoter has been shown to drive robust transgene expression in all tissues, permitting us to explore the consequences of widespread mutant VCP expression in a single animal including muscle, brain and bone which are tissues affected in IBMPFD (17–19). The disease-associated mutations R155H and A232E were introduced to wild-type human VCP by site-directed mutagenesis. These represent the most common and most severe disease-causing mutations, respectively.

Founder mice were generated by pronuclear injection and screened by PCR genotyping of tail DNA, resulting in four lines of VCP-wild-type (VCP-wt), five lines of VCP-R155H and five lines of VCP-A232E mice. VCP expression was evaluated in each line by western blot analysis and expression-matched lines were chosen for further study. The transgenic lines evaluated and presented here correspond to VCP-wt#7, VCP-R155H#55 and VCP-A232E#93 (hereafter, referred to as VCP-wt, VCP-R155H and VCP-A232E, respectively). Western blot analysis of VCP protein levels from muscle, brain and bone in these animals shows expression of VCP at 2–3-fold relative to endogenous levels (Fig. 1A). The animals were backcrossed onto the C57/B6 background, yielding the expected Mendelian ratios of transgene positive pups and F3 progeny were analyzed for evidence of the IBMPFD phenotype.

As we expected in a model of this adult-onset disorder, wild-type and mutant mice developed normally initially, but both VCP-R155H and VCP-A232E mice began to show adult-onset weight loss at ∼9 months of age and continued to decline in weight relative to their non-transgenic and VCP-wt counterparts (Fig. 1B). Beginning at 3–6 months of age, some VCP-R155H and VCP-A232E mice show a hind-limb clasping phenotype (Fig. 1C), which increased in severity and penetrance over time (Supplementary Material, Fig. S1A and B). This dyskinetic clasping posture is present in numerous mouse models of neurodegenerative disease and is a non-specific indicator of CNS pathology (20,21). Mice were followed until 15 months of age, and both VCP-R155H and VCP-A232E mice demonstrated a statistically significant decrease in survival as seen by Kaplan–Meier analysis (Fig. 1D). End-stage disease was characterized by a brief period of rapid weight loss, often accompanied by hind-limb paresis and animals were euthanized when weight loss reached 20% of maximal body weight or when decreased hind limb mobility hindered feeding and watering behaviors.

VCP mutant mice develop muscle weakness and histopathological signs of IBM including rimmed vacuoles and TDP-43 and ubiquitin-positive pathology

To determine whether mice expressing VCP-R155H and VCP-A232E would develop an IBM phenotype, mice were monitored for signs of muscle weakness by analysis of grip-strength using the well-established hanging wire test. Briefly, mice were suspended by their front limbs from a wire and the latency to fall was recorded with a maximum of 200 s permitted. Mice were tested every 4 weeks beginning at weaning. By 16 weeks of age, VCP-A232E mice showed a significant deficit in hanging wire performance compared with wild-type and non-transgenic controls (Fig. 2A). By 20 weeks of age, both VCP-A232E and VCP-R155H mice showed significant deficits in hanging wire performance. The earlier onset of muscle weakness in VCP-A232E mice is in accordance with

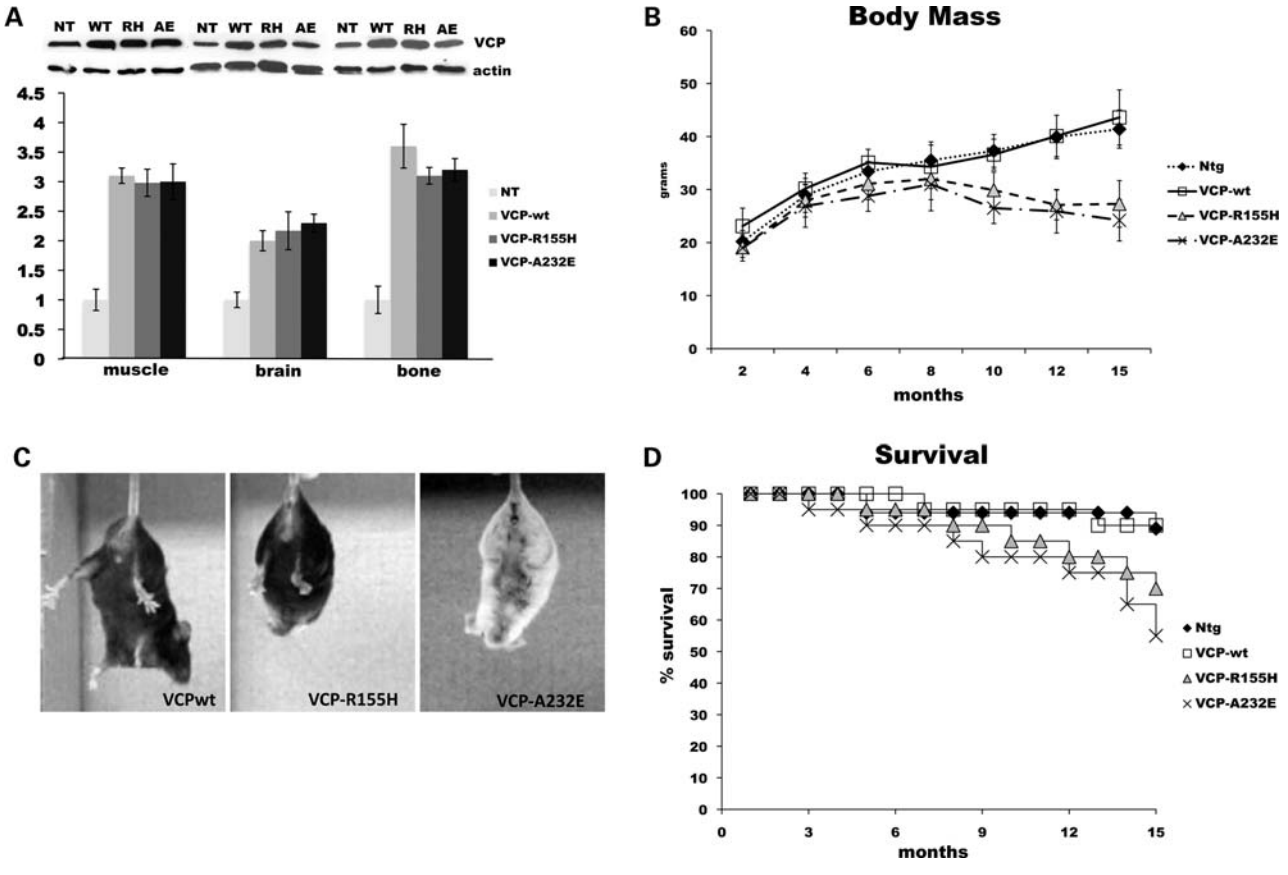

Figure 1. Generation of a mouse model of IBMPFD. (**A**) Tissue lysates from 8-week-old male mice were isolated from muscle, brain and bone and VCP protein levels were measured by western blotting with a monoclonal VCP antibody. Quantification of bands from three separate experiments reveals ~2-fold transgenic VCP expression relative to endogenous. (**B**) Mice were weighed every 2 months (only males are shown) and begin to show statistically significant weight loss at 8 months of age for VCP-A232E mice and 10 months of age for VCP-R155H. (**C**) When suspended by the tail, VCP mutant mice demonstrate the classical clasping response with both fore and hind limbs. (**D**) 18 non-transgenic mice and 20 mice from each VCP transgenic genotype were followed longitudinally for 15 months. Kaplan–Meier analysis shows that both VCP-A232E and VCP R155H lines show increased mortality relative to wild-type or non-transgenic controls ($P < 0.05$). Survival was analyzed by Kaplan–Meier, and body mass was analyzed by one-way ANOVA followed by *post hoc* Tukey's *t*-test.

the clinical presentation of the A232E mutations in humans, in which a more severe phenotype has been reported (22).

Histological analyses of quadriceps and gastrocnemius muscle taken from 9-month-old animals showed evidence of myogenic myopathy including irregular fiber size, centralized nuclei and inflammatory infiltrates (Fig. 2B–G and data not shown). In addition, modified Gomori trichrome staining revealed the presence of rimmed vacuoles in muscle from both VCP-R155H and VCP-A232E mice (Fig. 3E and data not shown), a hallmark of the degeneration seen in IBMPFD muscle, as well as sporadic IBM and other hereditary forms of IBM (23,24). Immunohistochemical examination of muscle from IBMPFD patients shows TDP-43 pathology in the form of cytoplasmic aggregates (25,26). Consistent with these observations, we observed cytoplasmic accumulation of TDP-43 in muscle from both VCP-R155H and VCP-A232E mice (Fig. 3A–D). Immunostaining of serial sections revealed that these cytoplasmic accumulations of TDP-43 are also ubiquitin-positive (Fig. 3F). Despite robust transgene expression as determined by western blot analysis, liver, kidney, spleen and intestine from IBMPFD mice appear histologically normal, and blood chemistries reveal no evidence of liver or kidney dysfunction (Supplementary Material, Fig. S3). VCP/p97 transgene expression was distributed evenly throughout the muscle fibers, and no correlation was seen between the level of VCP expression per fiber and fiber integrity (Supplementary Material, Fig. S4).

Ultrastructural analysis of quadriceps and gastrocnemius muscle from VCP-R155H and VCP-A232E mice by TEM revealed severely disorganized sarcomeres scattered among more normal-appearing sarcomeres best appreciated in the longitudinal plane (Fig. 4A–D and data not shown). When examined in cross-section, sarcomeres from VCP mutant mice frequently showed loss of myofilament integrity (Fig. 4E and F). These myofiber abnormalities in VCP-R155H and VCP-A232E mice were accompanied by abnormal mitochondria scattered among more normal-appearing mitochondria. The abnormal mitochondria exhibited marked pleioconia and megaconia (Fig. 4C and D).

VCP has been implicated as playing an important role in regulating myofibrillogenesis through regulating the steady state levels of the muscle-specific chaperone protein Unc45b (27). Dysregulation of Unc45b levels leads to defects if myofibrillogenesis in multiple animal model systems (28,29).

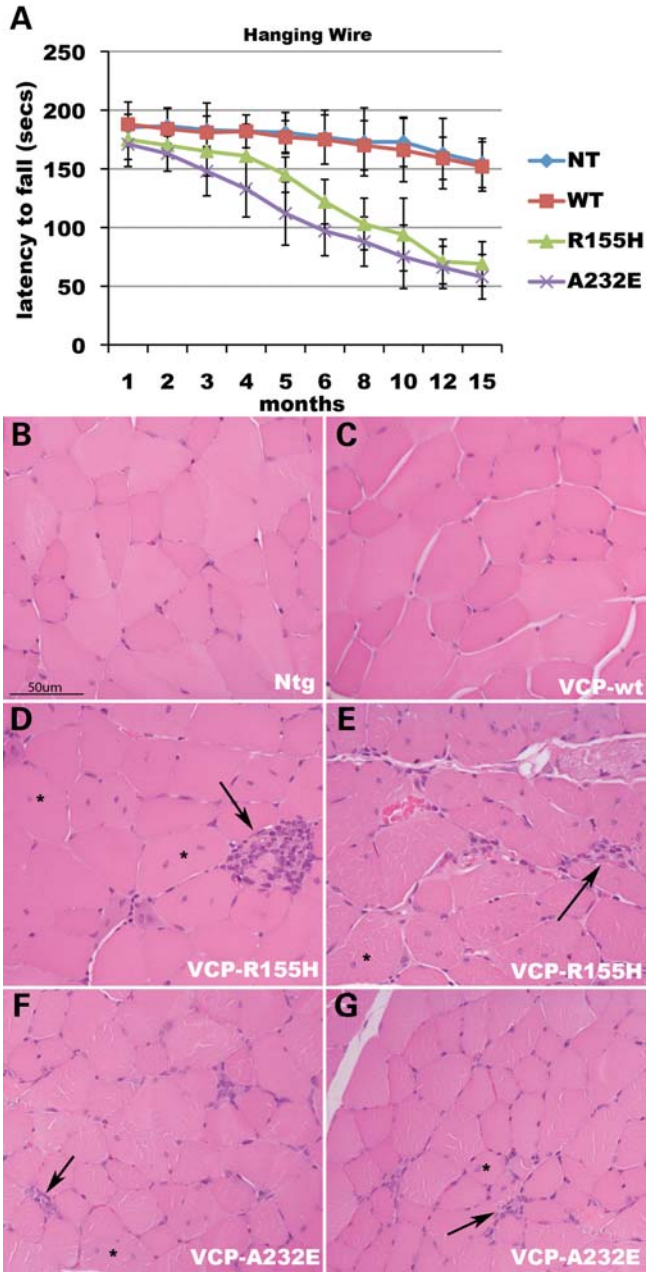

Figure 2. VCP mutant mice develop muscle weakness and histological signs of a myogenic pattern of myopathy. (**A**) Hanging wire performance in male mice is significantly reduced ($P < 0.01$) in VCP-A232E mice by 4 months, and is significantly reduced in VCP-R155H by 6 months. (**B**–**G**) H and E staining of paraffin embedded quadriceps muscle from 9-month-old paraformaldehyde-perfused non-trasngenic (B) VCP-wt transgenic (C) VCP-R155H (D and E) and VCP-A232E (F and G) mice shows normal muscle morphology in VCP-wt tissue, but marked signs of degeneration in both mutant lines including centralized nuclei (asterisks), irregular fiber size and inflammatory infiltrates (arrows).

Disease-causing mutations in VCP were shown to stabilize Unc45b levels *in vitro*, implicating this as a contributing factor to myopathy in IBMPFD (29). Consistent with these data, muscle lysates from VCP-R155H and VCP-A232E mice showed significantly increased steady-state levels of Unc45b protein compared with wild-type and non-transgenic controls, with a more prominent stabilization observed in the more severely affected VCP-A232E muscle (Fig. 4G). These increased levels of Unc45b are consistent with a mechanism in which overactive myosin remodeling contributes to the loss of the sarcomere integrity seen by TEM.

VCP mutant mice develop behavior abnormalities as well as TDP-43- and ubiquitin-positive pathology

IBMPFD patient brain tissue is characterized by ubiquitin- and TDP-43-positive pathology in the form of intranuclear and cytoplasmic inclusions and accumulation in dystrophic neurites (30). TDP-43 is also the major disease protein in the ubiquitinated inclusions characteristic of both sporadic and familial forms of frontotemporal lobar degeneration (FTLD-TDP) as well as ALS. In these diseases, TDP-43 redistributes from the nucleus to cytoplasmic aggregates (15,31). Brains harvested from VCP transgenic mice at 4, 6, 8, 10, 12 and 14 months of age showed no overt signs of degeneration by hematoxylin and eosin stain. First apparent at 14 months of age; however, immunohistochemical staining for TDP-43 demonstrated nuclear clearance and cytoplasmic accumulation in widespread brain regions, but not in the hippocampus (Fig. 5) despite strong transgene expression in this brain region (Supplementary Material, Fig. S3A). Quantification of nuclear clearance in cortex and spinal cord motor neurons reveals that $>10\%$ of cells in cortex and $\sim 5\%$ of neurons in spinal cord lack nuclear TDP-43 immunostaining (Supplementary Material, Fig. S5). At this age areas of mild gliosis particularly in the cerebellum were also observed (data not shown). Double-labeled immunofluorescence showed that these cytoplasmic accumulations of TDP-43 are ubiquitin-positive, thereby recapitulating a prominent feature of FTLD-TDP and IBMPFD neuropathology (Fig. 6A–I). However, no nuclear inclusions immunopositive for TDP-43 or ubiquitin were observed.

We next sought to characterize the behavioral phenotype of our VCP mice. Increased levels of anxiety have been reported in numerous transgenic mouse models of dementia including models of Alzheimer's disease and tauopathies (32,33) and so we monitored the VCP mutants for signs of anxiety-associated behavior. To measure anxiety, we evaluated behavior of non-transgenic, VCP-wt, VCP-R155H and VCP-A232E mice on an elevated zero maze at 12, 16, 20, 24 and 48 weeks of age. For testing with an elevated zero maze, an animal is placed on a circular platform that is divided into four quadrants. The quadrants alternate between closed quadrants that are enclosed by 8-in. walls and open quadrants with only a small lip. The amount of time that an animal spends in each quadrant is recorded, and significantly increased time spent in closed quadrants is associated with increased anxiety (34). Beginning at 16 weeks of age in VCP-A232E mice and 20 weeks of age in VCP-R155H mice, we observed significantly increased anxiety relative to their wild-type and non-transgenic counterparts (Fig. 6J). Importantly, VCP mutant mice showed no changes in locomotor activity at this age that would confound the results (Supplementary Material, Fig. S2B). The degree of anxiety was stable after 20 weeks and did not increase at later time points (Supplementary Material, Fig. S2A).

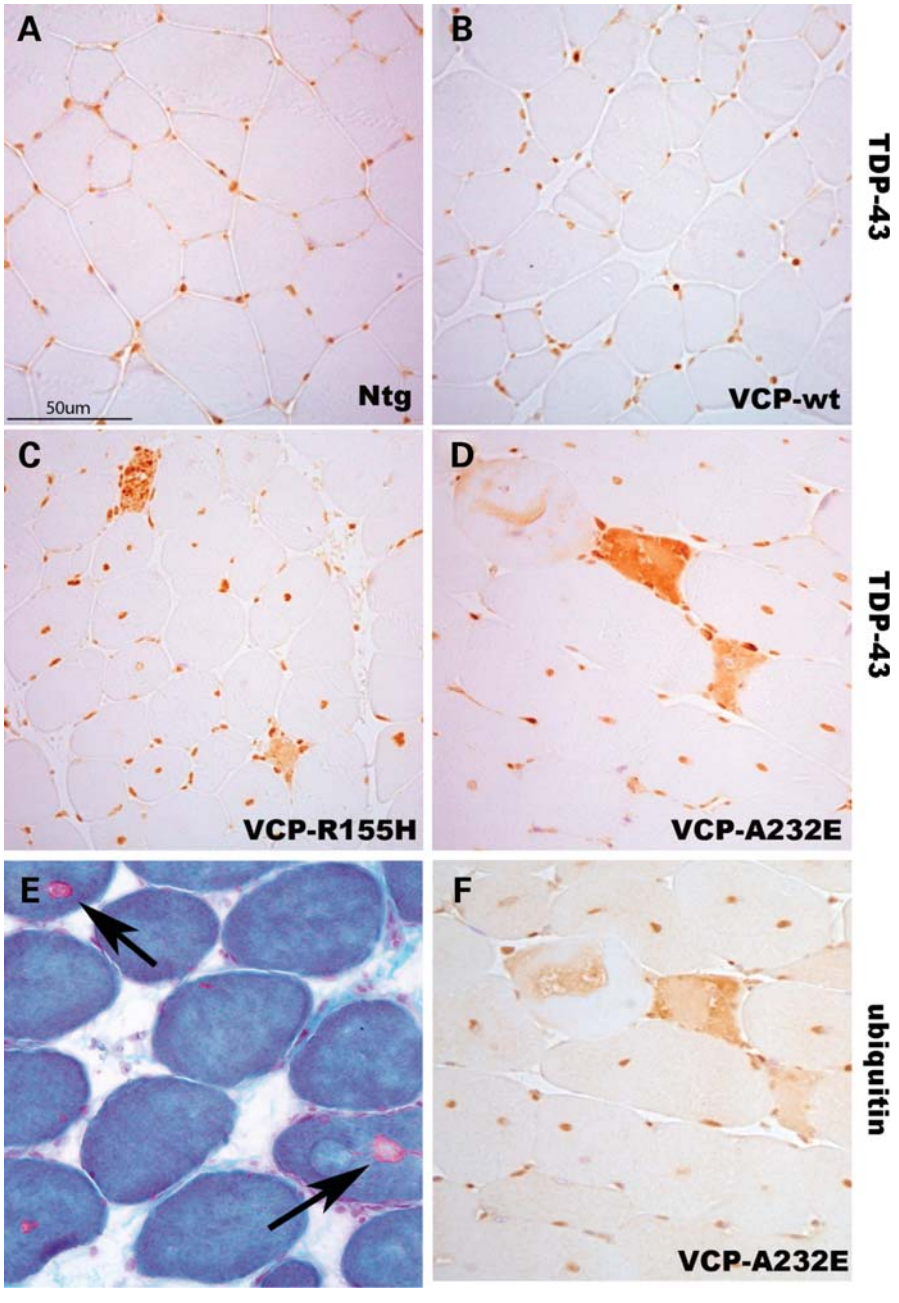

Figure 3. VCP mutant mice show skeletal muscle TDP-43 pathology and rimmed vacuoles evident with Gomori trichrome staining. (**A**) Immunostaining of paraffin embedded quadriceps from non-transgenic (A), VCP-wt (**B**), VCP-R155H (**C**) and VCP-A232E (**D**) animals at 9 months with a polyclonal TDP-43 antibody shows normal nuclear staining in non-transgenic and VCP-wt tissues, but demonstrates strong cytoplasmic accumulation in both VCP-R155H and VCP-A232E tissues (C and D). (**F**) Staining of serial sections shows that these cytoplasmic TDP-43 accumulations are also ubiquitin positive. (**E**) Modified trichrome staining in A232E quadriceps shows the presence of rimmed vacuoles (arrows), a hallmark of IBM pathology.

At 14 months of age, when TDP-43 pathology was first appreciated, we assessed the animals' declarative memory using a novel object recognition task. This task was chosen because it is considered to be primarily an assessment of hippocampal-independent learning and memory, and the hippocampus appears to be spared in IBMPFD brains (35). Moreover, novel object recognition deficits have been reported in multiple mouse models of FTD (36,37). For this task, the animals were placed in a large enclosure containing two objects. The animals were allowed to explore the area, and investigation of the two objects was recorded. After an interval of 24 h, the animals were placed back in the training environment, with one of the original objects having been replaced by a novel object, and the number of visits to each object was again recorded. The ratio of novel object visits to training object visits was calculated, with no apparent preference for either object resulting in a ratio of 1. At 24 h post-training, normal mice show a preference for the novel object

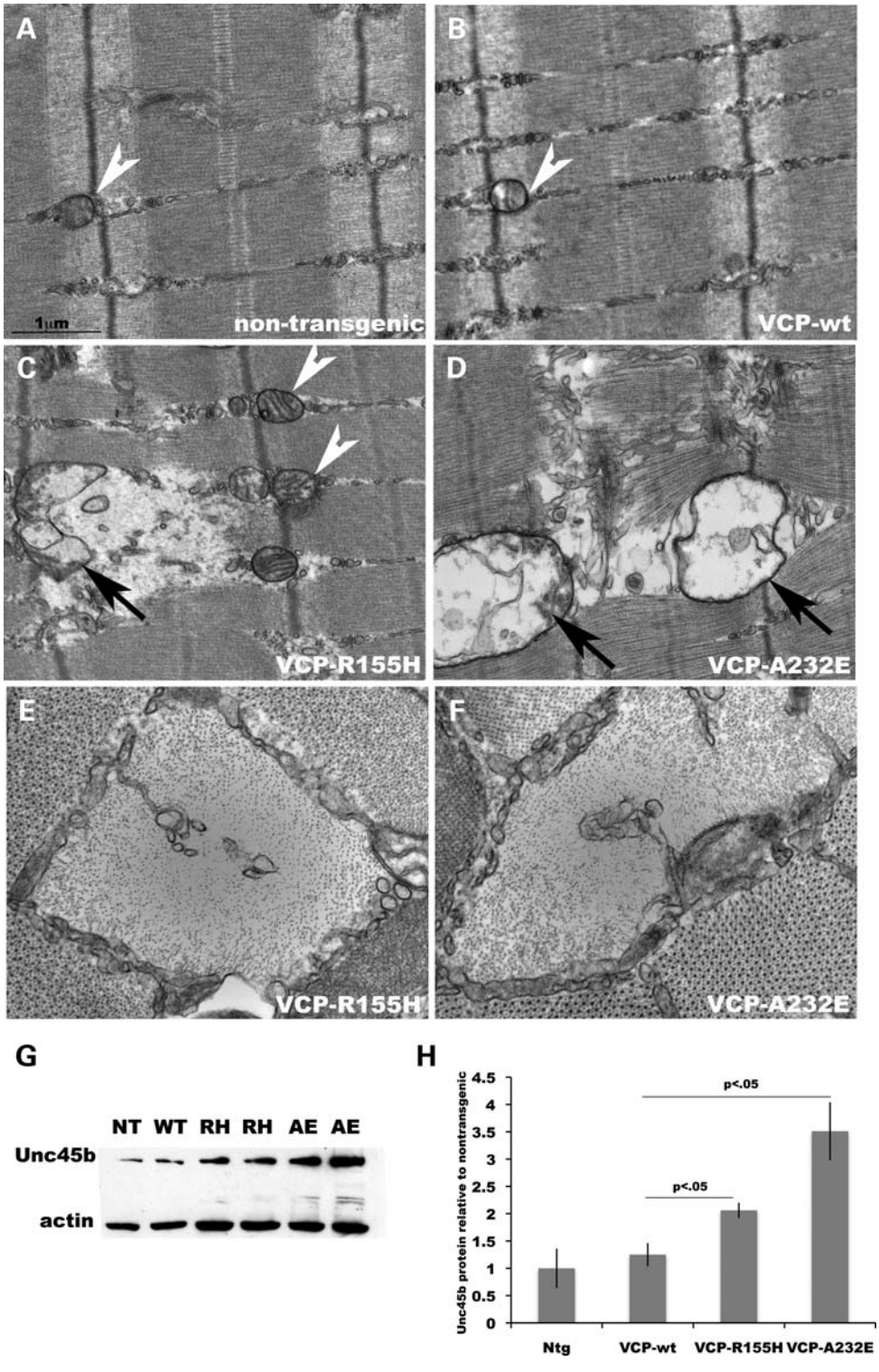

Figure 4. VCP mutant mice show loss of myosin fiber integrity and stabilization of the myosin chaperone protein Unc45b. (**A**–**D**) TEM from quadriceps muscle (20 000×) shows marked degeneration of the normal sarcomeric structure in both VCP-R155H (C) and VCP-A232E (D) muscle, and also the accumulation of swollen, severely degenerated bodies that can be identified as mitochondria by their few remaining intact cristae (arrows). For comparison, normal mitochodria are marked with white arrow heads. Muscle from non-transgenic and VCP-wt animals appears normal at this age (A and B). (**E** and **F**) Cross-sectional views of mutant muscle show dramatic loss of myosin fibers and accumulation of vacuoles. (**G**) Western blotting of skeletal muscle lysates from age-matched animals (12 months) shows an increase in Unc45b protein from two separate R155H and A232E animals compared with VCP-wt and non-transgenic controls. (**H**) Quantitative image analysis of Unc45b western blots from three separate experiments shows significant stabilization of Unc45b protein levels compared with actin loading controls in VCP-R155H and VCP-A232E mice compared with VCP-wt or non-transgenic control animals.

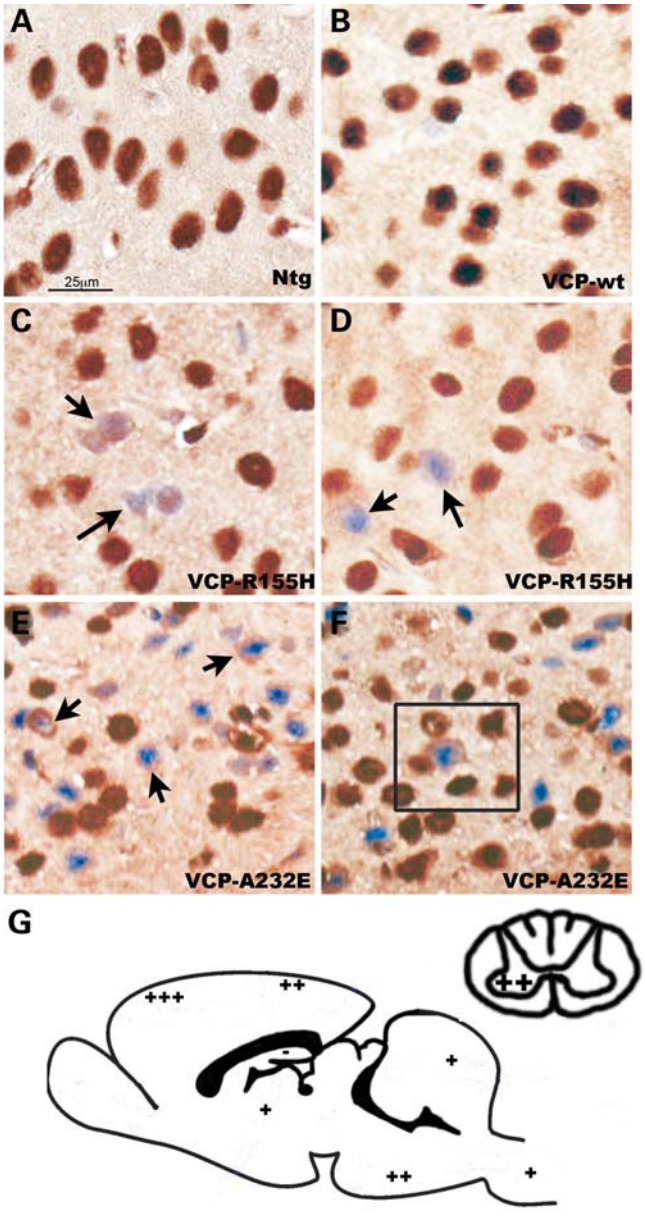

Figure 5. IBMPFD transgenic mice develop ubiquitin- and TDP-43-positive neuropathology. (**A**–**D**) Immunohistochemistry on paraffin embedded brains from 14-month-old animals reveals loss of the normal nuclear TDP-43 staining patterns in neurons from cortical layer two-third in both VCP-R155H (C and D) and VCP-A232E (**E** and **F**) brains compared with the normal nuclear staining seen in non-transgenic (A) and VCP-wt (B) brains. Occasionally, especially in brains from VCP-A232E animals, this nuclear clearance is accompanied by cytoplasmic accumulation of tdp-43 (F inset). (**G**) Two separate observers, who then ranked the prominence of nuclear clearance, assessed nuclear clearance of TDP-43. Areas of the brain where no clearance was seen are represented as −. Areas that contained nuclear clearance were graded, with +++ being prominent nuclear clearance (>10% of cells counted), ++ being rated as occasional (5–10%) and + as rare, but present (<1–5%). Both observers agreed that the nuclear clearance was most prominent in frontal cortex and was completely absent from hippocampus. Moderate nuclear clearance was seen in the pons, brainstem and lumbar spinal cord.

by visiting it more frequently than the training object (38). At training, all mice showed no apparent preference for either object, producing ratios of ∼1 (Fig. 6K). When presented with the novel object 24 h post-training, the VCP mutant mice showed significantly decreased exploration of the novel object relative to wild-type or non-transgenic animals, suggestive of impairment in non-hippocampal learning and memory performance. Thus, VCP mutant mice exhibit TDP-43 neuropathology and deficits in multiple neurological tasks.

VCP mutant mice develop severe osteopenia and focal pagetic lesions

Paget's disease of bone is a metabolic bone disorder. The pathogenic process begins with hyperactive bone resorption by osteoclasts. This activity is followed by a compensatory increase in osteoblast activity leading to the increased production of poorly formed bone. Over an extended period of time this process results in bone deformities, pain and propensity to fracture. The PDB seen in IBMPFD patients has a much earlier onset than sporadic PDB, but otherwise follows a classic pattern of presentation (39).

At 13 months of age, we evaluated non-transgenic, VCP-wt, VCP-R155H and VCP-A232E mice for signs of skeletal by X-ray microtomography (μCT) scan at a resolution of 16 μm. The left and right femur from three male mice of each genotype were dissected and scanned, and quantitative volumetric analysis was performed. Renderings of sagittal sections through the mid-shaft of the femur showed dramatic loss of trabecular structure in both distal and proximal femur (Fig. 7A and B). Quantification showed decreased trabecular number and thickness as well as increased trabecular spacing and Euler number in VCP mutants (Fig. 7C). This loss of trabecular structure in VCP mutant mice was also seen throughout the vertebral column at this age (data not shown). In the longitudinal μCT scans, it is apparent that in addition to the osteopenia, VCP mutants show occasional sclerotic lesions studding the internal surface of the cortical bone (Fig. 7A, arrows) as well as focal regions of radiolucency that are apparent in 'red glass' renderings of distal femur (Fig. 7B, arrows) which are indicative of focal areas of decreased bone density. Solid color volume renderings show areas of hypomineralization in patchy regions of cortical bone in the distal epiphysis (Supplementary Material, Fig. S5).

Cells expressing mutant VCP show increased activation of NF-κB

VCP/p97 regulates a plethora of cellular processes including ubiquitin-dependent protein degradation, stress responses, nuclear envelope reconstruction and Golgi and endoplasmic reticulum assembly (40). At present it is unclear which of these processes are impacted by disease-causing mutations in VCP/p97 and it is likely that multiple normal functions are affected. Among the well-characterized roles of VCP is control of the NF-κB pathway through regulation of ubiquitin-dependent degradation of IκB-α (41–43). The NF-κB signaling pathway plays a key role in osteoclastogenesis and is known to be a major player in PDB (44). Osteoclast precursors express receptor activator of NF-κB (RANK), which is activated by binding of the ligand RANK-L, produced by osteoblasts. RANK-L binding to RANK initiates a signaling cascade that results in activation of NF-κB resulting in increased

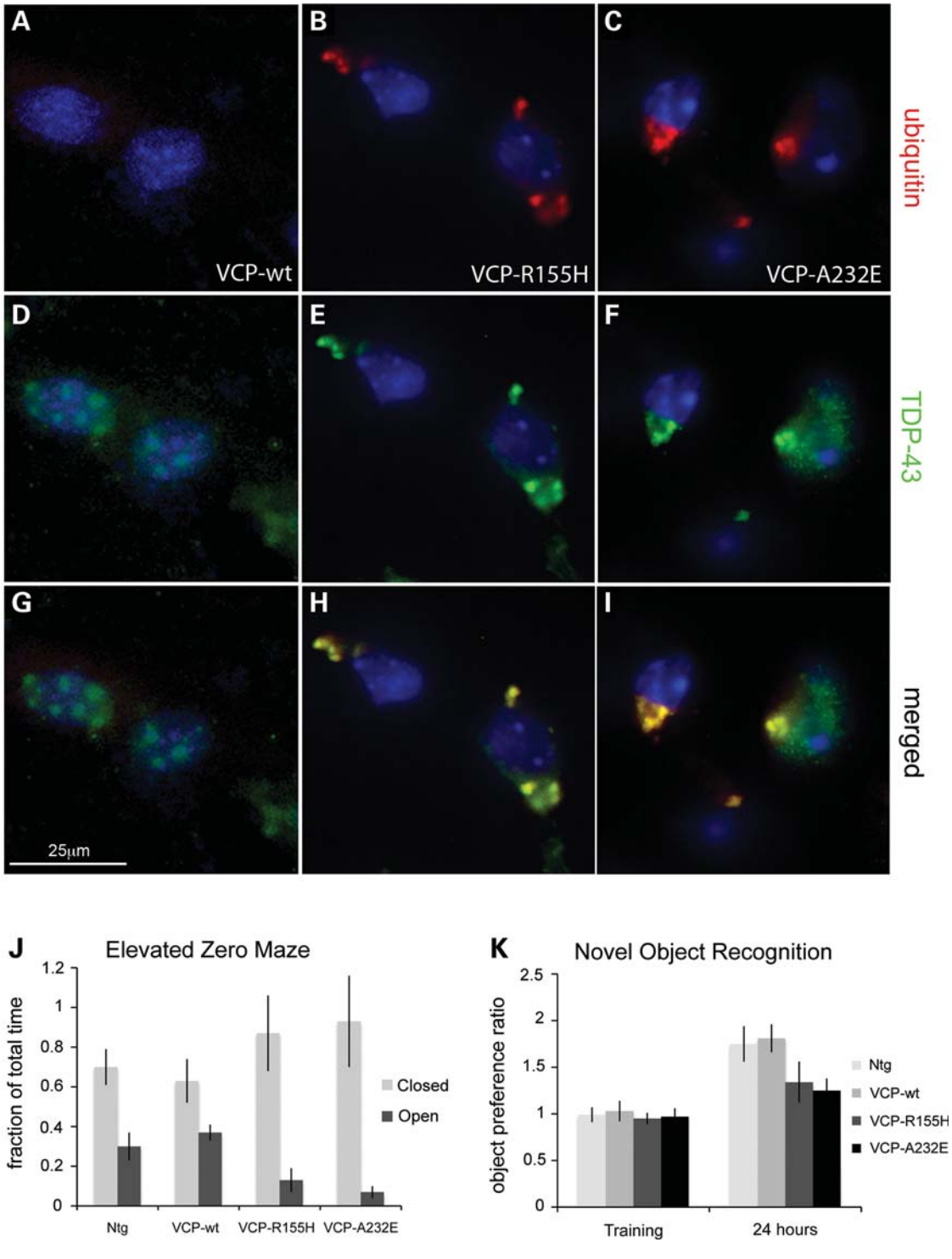

Figure 6. VCP mutant neurons show co-localization of cytoplasmic TDP-43 and ubiquitin, and behavioral assays reveal anxiety and memory defects. (**A**–**I**) Double-label immunohistochemistry on frozen sections of mouse cortex reveals the accumulation of TDP-43 (green) and ubiquitin (red) immunopositive cytoplasmic inclusions in both VCP-R155H (B, E, H) and VCP-A232E (C, F, I) mice at 14 months. Nuclei are visualized in blue with DAPI. No such staining was present in VCP-wt brains (A, D, G), which retain their normal nuclear TDP-43 staining and had no detectable ubiquitin positive aggregation. (**J**) When analyzed by elevated zero maze, both VCP-R155H and VCP-A232E animals spend increased amounts of time in the closed arms of the maze, indicating increased anxiety behavior (J black bars) χ^2 analysis shows that there is a significant effect of mutant VCP on the distribution of time spent in the open versus the closed quadrants ($P < 0.01$) and *post hoc t*-test revealed no significant difference between the VCP-R155H and VCP-A232E animals. (**K**) At 14 months of age when tested with a novel object recognition paradigm, mutant mice tested with a trial interval of 24 h, show decreased novel object preference (object ratio <1) compared with non-transgenic and VCP-wt controls.

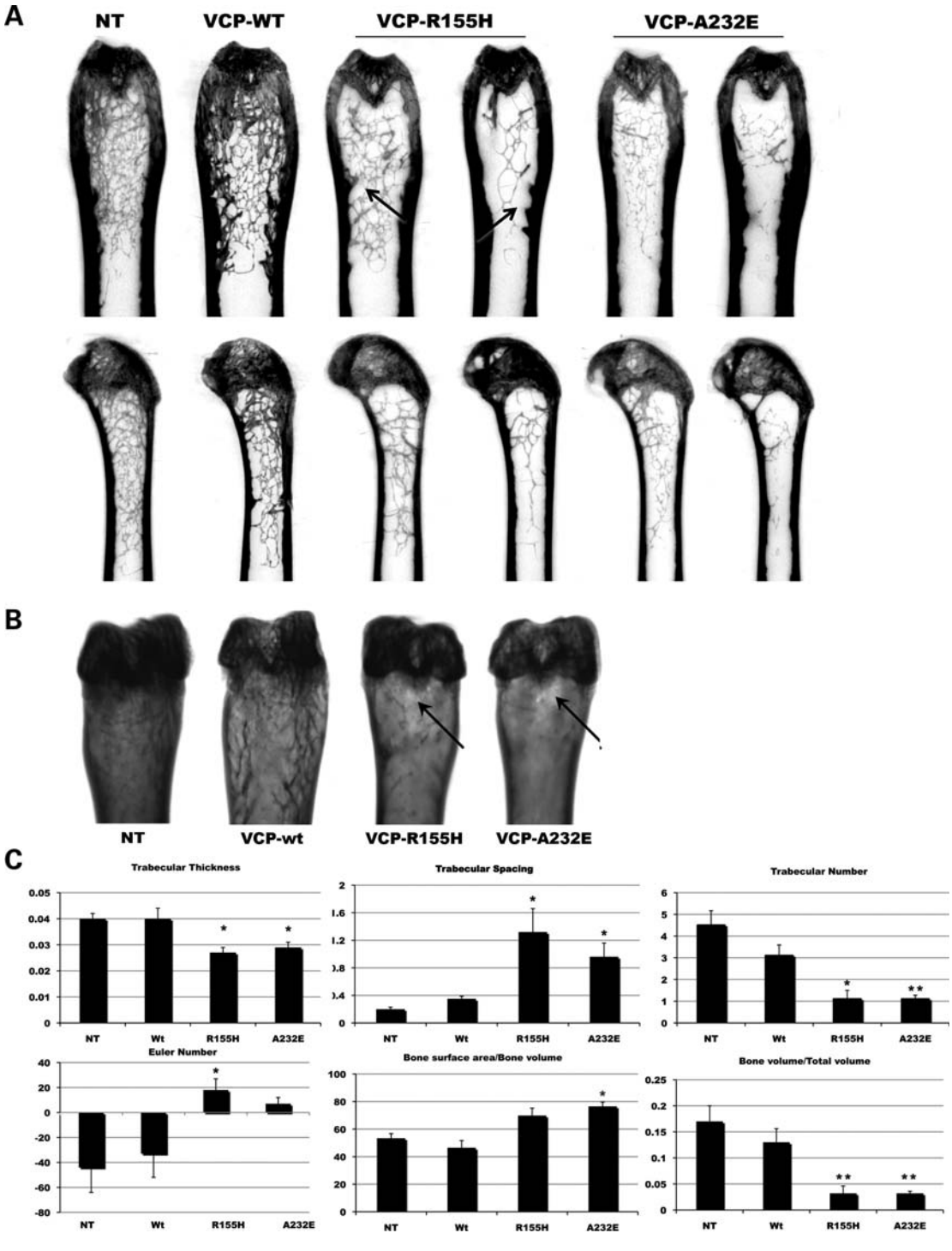

Figure 7. VCP mutant mice show loss of trabecular bone and focal Pagetic lesions. (**A**) High resolution μCT scans of femur at 13 months shows loss of trabecular bone in VCP-R155H and VCP-A232E animals compared with VCP-wt and non-transgenic controls. (**B**) In addition to the obvious loss of trabecular structure, occasional focal areas of thickening cortical bone can be seen (arrows). Red glass renderings show areas of decreased density in cortical bone (arrows). (**C**) Quantitative volumetric assessment of distal trabecular structure shows significant changes on all metrics captured, including decreased trabecular number, increased trabecular spacing, decreased trabecular thickness and more positive Euler number for VCP mutants compared with VCP-wt and non-transgenic controls (data were analyzed by one-way ANOVA followed by *post hoc t*-test between groups. $^{*}P < 0.05$, $^{**}P < 0.01$ when compared with non-transgenic).

transcription of osteoclastogenic genes. Two familial forms of PDB are caused by mutations that impact activation of NF-κB by RANK-L, including SQSTM1/p62 and osteoprotegrin, which inhibits RANK-L signaling. PDB-causing mutations in either of these genes result in increased NF-κB activity, hyperactive osteoclasts and increased bone resorption (45–48).

In contrast to the role of NF-κB in bone disease, the role of NF-κB in muscle disease has only recently been illuminated and is now implicated as a factor in muscle atrophy in multiple disease states (49). For example, mice expressing muscle-specific, constitutively active IKK ('MIKK mice') show increased basal NF-κB activity, and most importantly, increased NF-κB-dependent muscle degeneration following disuse. Increased NF-κB signaling leads to increased transcription of the muscle-specific E3 ligase URF1/TRIM63, which leads to the ubiquitination and subsequent degradation of myosin fibers, and loss of Murf1 partially rescues the muscle wasting (50). Thus, hyper-activation of NF-κB signaling has been implicated as an important contributor to degeneration of both skeletal muscle and bone, two tissues that are affected in IBMPFD, and provides a possible common disease mechanism.

VCP modulates the NF-κB signaling pathway by regulating the degradation of IκB-α. IκB-α normally retains NF-κB in an inactive state in the cytoplasm. In response to TNF-α or RANK-L binding, IκB-α is phosphorylated and then ubiquitinated and subsequently degraded by the proteasome in a VCP-dependent manner (41). This degradation of IκB-α frees NF-κB to be activated by phosphorylation and then translocate to the nucleus. VCP knockdown leads to accumulation of IκB-α and decreased activation of NF-κB (43). Thus, we hypothesized that the pathogenic mechanism of IBMPFD may involve increased clearance of IκB-α and consequently increased the downstream activation of NF-κB with pathological consequences in muscle and bone.

To test this hypothesis, we evaluated NF-κB signaling in C2C12 cells over-expressing wild-type or VCP-A232E. We treated the cells with TNF-α (100 ng/ml) for 0, 5 or 30 min, and monitored protein levels of IκB-α and phosphorylated NF-κB by western blot. As expected, cells transfected with VCP-wt showed increased clearance of IκB-α in response to TNF-α, but the recovery of IκB-α followed roughly the same kinetics as control cells, returning to near normal levels by 30-min (Fig. 8A and B). In contrast, cells transfected with VCP-A232E showed significantly greater clearance of IκB-α that persisted through the 30-min time point (Fig. 8A and B). Our evaluation of NF-κB activation revealed a consistent pattern. Cells transfected with VCP-A232E showed significantly increased levels of phosphorylated NF-κB (P-NF-κB) following TNF-α treatment, and the increase persisted at 30-min (Fig. 8A and B).

To determine whether this apparent increase in NF-κB signaling had functional consequences, cells were co-transfected with VCP and a luciferase reporter construct driven by tandem repeats of the NF-κB response element. Twenty-four hours post-transfection, we treated C2C12 cells with increasing concentrations of TNF-α for 16 h. Cells transfected with VCP-A232E showed significant increases in basal NF-κB activity, as well as a leftward shift of the dose-response curve indicating increased sensitivity to TNF-α (Fig. 8C). At higher doses of TNF-α, cells expressing either VCP-wt or VCP-A232E showed increased luciferase activity compared with control cells, but were not statistically different from each other (Fig. 8C). These data implicate amplification of the NF-κB signaling pathway in the pathogenesis of IBMPFD and suggest the possibility of common underlying mechanisms of pathogenesis in multiple tissues affected in IBMPFD.

DISCUSSION

IBMPFD is a devastating multisystem degenerative disease, and although several years have passed since genetic studies have identified mutations in VCP/p97 as the cause of this dominantly inherited disease, relatively little progress has been made identifying the molecular mechanism(s) of pathogenesis. VCP/p97 activity is vital to a diverse array of cellular activities and it is likely that multiple perturbations are initiated by disease-causing mutations and that pathogenesis is multi-factorial and complex. Moreover, it is quite possible that molecular pathogenesis differs in different tissues. A prior mouse model targeted mutant VCP expression to muscle and characterized degeneration in this tissue, but there remained a need for an animal model faithfully recapitulating the full spectrum of pathologies seen in human IBMPFD. Here, we have presented the development and characterization of transgenic mice in which ubiquitous expression VCP carrying either of two distinct disease-causing mutations (R155H or A232E) faithfully recapitulates the complete IBMPFD phenotype, including involvement of muscle, brain and bone.

Characteristics of the IBMPFD mice

Muscle weakness in VCP-R155H and VCP-A232E mice becomes significant at 20 and 16 weeks, respectively, and is slowly progressive (Fig. 2A). Histopathological examination reveals classical features of IBM including myogenic atrophy accompanied by inflammatory infiltrate and rimmed vacuoles (Figs 2B–G and 3E). Moreover, myopathy in the VCP-R155H and VCP-A232E mice exhibits TDP-43 pathology that overlaps ubiquitin pathology (Fig. 3) consistent with observations in human sporadic and inherited IBM (26,51,52). Ultrastructural analysis of degenerating muscle reveals loss of myofiber integrity in some sarcomeres accompanied by markedly swollen, degenerating mitochondria (Fig. 4C and D). VCP-R155H and VCP-A232E transgenic mice develop behavioral abnormalities including increased anxiety that becomes significant at 20 and 16 weeks, respectively, similar in age of onset to muscle weakness (Fig. 6J and Supplementary Material, Fig. S2). The mutant mice also develop a deficit in novel object recognition at 14 months (Fig. 6K). Neuropathological examination revealed widespread redistribution of TDP-43 from the nucleus to cytoplasmic aggregates, but no nuclear inclusions of TDP-43 (Fig. 5). Moreover, double labeling indicated that cytoplasmic TDP-43 was immunopositive for ubiquitin (Fig. 6). Radiological evaluation of the skeletons revealed that VCP-R155H and VCP-A232E transgenic mice develop profound osteopenia, with some focal areas of increased radiolucency and other areas of increased bone (Fig. 7). Expression of mutant VCP in other tissues also—including heart, liver, kidney, spleen and intestine—was not associated with pathology, consistent with the selective vulnerability of muscle, brain and bone

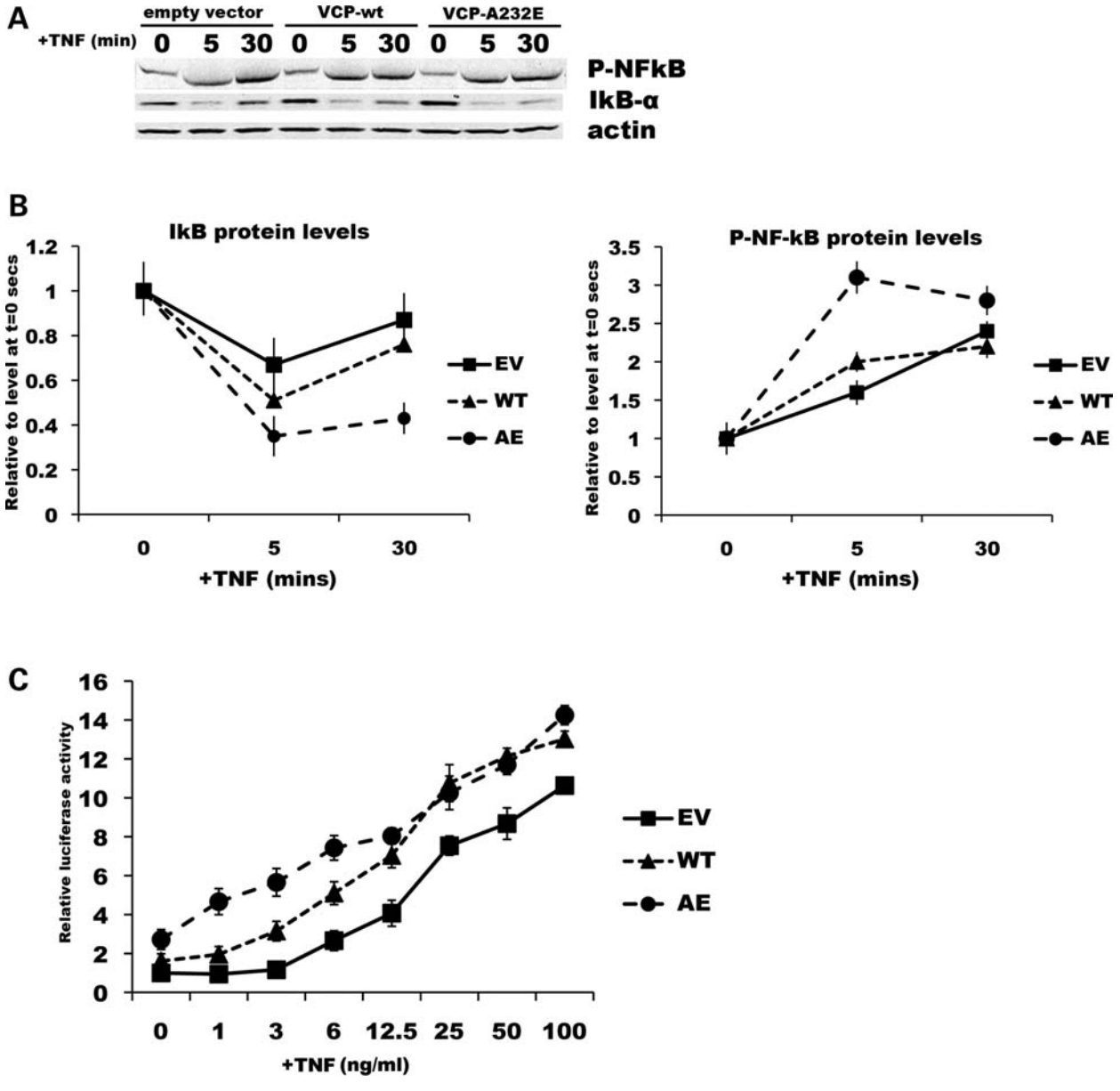

Figure 8. VCP mutant myoblasts show increased NF-κB signaling. (**A**) C2C12 myoblasts were transiently transfected with wild-type or mutant VCP constructs, and treated with TNF-α (100 μg/ml) for 5 and 30 min. Cells were lysed and analyzed by western blot. Cells transfected with VCP-A232E show increased clearance of IκB-α at 5 min, and levels are slower to return to normal compared with empty vector and VCP-WT controls. A corresponding increase was seen in phosphorylated NF-κB protein levels. (**B**) Graphical representation of IκB-α and NF-κB protein levels relative to actin as quantified by ImageJ densitometry shows significant changes in the rate of recovery of IκB-α levels in VCP-A232E lysates and significant increases in activation of NF-κB in response to TNF-α. (**C**) C2C12 myoblasts were co-transfected with wild-type or mutant VCP and an NF-κB luciferase reporter construct, and exposed to increasing concentrations of TNF-α (0–100 μg/ml) overnight. Luciferase activity shows a leftward shift in the TNF-α dose response curve, with increased NF-κB driven luciferase activity at lower doses. These data were analyzed by one-way ANOVA followed by *post hoc* Tukey's *t*-test to determine differences between groups.

observed in patients with IBMPFD. This is the first complete mouse model of IBMPFD and will be an important tool in advancing our understanding of disease pathology. Furthermore, this model may be an important tool for understanding sporadic forms of IBM, PDB and FTD-TDP.

Insights into pathogenesis of IBMPFD

VCP/p97 regulates the ubiquitin-dependent degradation of a wide variety of proteins that themselves are key regulators of discrete biological processes. In this way, VCP/p97 enables hierarchical control of numerous biological processes by the ubiquitin-proteasome system. Disease pathogenesis may involve very subtle alteration of native VCP/p97 function, rather than an entirely novel gain of function or dominant negative mechanism. Because so many of the known VCP/p97 interacting proteins are themselves involved in cellular signaling cascades, these small changes in VCP/p97 function may be amplified throughout the cell, leading to wide-spread changes in the cellular environment.

All of the IBMPFD-causing mutations affect residues that may influence interaction of the N-terminal domain of VCP/p97 with the D1 region of the protein (53). Thus, mutations may influence VCP/p97 binding to adaptor proteins. Specifically, we hypothesize that IBMPFD-causing mutations favor association with some adaptors, which may contribute to pathogenesis through a gain-of-function mechanism. Concomitantly, IBMPFD-causing mutations may attenuate the interaction with other adaptors, contributing to pathogenesis through a partial loss-of-function mechanism. Consistent with this hypothesis, biochemical analysis of VCP mutants R155H and A232E demonstrate that mutant protein appropriately forms hexamers. Moreover, these mutants show ~3-fold increase in ATPase activity and also enhanced ATPase activation in response to elevated temperature (54), consistent with amplification of a normal VCP function.

This hypothesis further predicts that mutations in VCP/p97 may have wide-ranging impact on multiple, distinct cellular functions, whereas leaving some VCP functions intact. Consistent with this hypothesis, we recently showed that disease mutations impair an essential function of VCP in regulating autophagy, but do not impair VCP function in endoplasmic reticulum-associated proteasomal degradation (13). In this study, we found evidence of additional VCP functions that are impaired and may contribute to the complex disease phenotype. For example, VCP/p97 works in complex with CHIP and UBE4B to regulate the steady state levels of the muscle chaperone Unc45b. Unc45b is a master regulator of myofibrillogenesis and altered Unc45b levels (either too much or too little) cause defects in myofiber integrity (27). We have found significantly increased Unc45b levels in the muscles from VCP-R155H and VCP-A232E mice, suggesting that this mechanism may contribute to myopathy in IBMPFD. VCP/p97 also regulates activity of the NF-κB signaling pathway through regulating degradation of IκB-α, possibly in complex with the SCF-like complex containing the E3 ligase beta-TrCP1 (55,56). We have shown that overexpression of mutant VCP is associated with amplification of signaling through the NF-κB pathway, implicating perturbation of this critical signaling pathway as also contributing to disease. Importantly, amplification of NF-κB signaling has been previously identified as the molecular defect underlying multiple genetic forms of PDB (44). More recently, as discussed earlier, amplification of NF-κB signaling has also been implicated as a potentially important contributor to muscle disease (49). Thus, amplification of the NF-κB signaling may be a common underlying mechanism of pathogenesis in multiple tissues affected in IBMPFD.

A significant challenge in future IBMPFD research will be to further untangle the contribution of individual perturbations caused by VCP mutations to tissue-specific disease manifestations, and we believe that the mouse model presented here provides an excellent resource in our further search for the molecular underpinnings of IBMPFD.

MATERIALS AND METHODS

Generation of transgenic mice

Human VCP cDNA was obtained from Origene. Disease-associated mutations R155H and A232E were introduced using the QuickChange Site-Directed Mutagenesis Kit (Stratagene) as directed. The cDNA was then subcloned into the SmaI site of pCX-A (a gift from Dr Albert R LaSpada). DNA was microinjected into male SJL pronuclei, which were then transferred to foster females. Founders were screened by PCR of tail DNA and positive founders were bred to C57/B6 animals to produce F2 progeny. Mice were housed according to the University of Pennsylvania's animal care policies.

Behavioral testing

Elevated zero maze. The zero maze (Med Associates) consists of a circular platform (6.1 cm width with a 40 cm inner diameter) that is equally divided into four quadrants. Two quadrants on opposite sides of the platform are enclosed by walls (20.3 cm high); the other two quadrants are open and bordered by a lip (0.6 cm high). The maze is elevated 72.4 cm above the floor and there is an overhead camera and tracking system to monitor activity of the mouse. Mice were placed with all four paws inside closed quadrant 1, facing into the closed quadrant. Each animal was allowed 5-min on the maze, and the maze was cleaned with 70% ethanol between animals. Trials were recorded on video, and an observer later scored the time spent in each of the four quadrants.

Hanging wire test. Mice were suspended by their forepaws from a metal wire (2 mm diameter) ~18 in. above a padded cage and latency to fall was recorded with a maximum of 200 s.

Novel object recognition. Six mice from each genotype were tested at 14 months of age. On day 1, the mice were acclimated to the training chamber for 5-min in the absence of any objects. On day 2, the animals were placed in the training chamber with two objects (a glass beaker and a block) for 5-min, and visits to each object as defined by a nose poke within 1 cm were recorded. Finally, on day 3 the animals were tested for their 24 h interval, and again were presented with their familiar object (glass beaker) and a novel object (striped block). An object preference ratio was recorded, defined as the time spent with the novel object divided by the time spent with the familiar object, meaning that equal preference would produce an object preference ratio of 1.

Histology

Mice were anesthetized followed by transcardial perfusion with 4% paraformaldehyde in 0.1 M phosphate buffer. Brain, bone and skeletal muscle were removed and post-fixed for 24 h. Tissues were either processed for paraffin embedding or saturated with 30% sucrose (w/v) before OCT embedding and cryostat sectioning at 4 mm.

Western blotting

Freshly isolated tissues were quickly frozen between two blocks of dry ice and immediately crushed and resuspended in 1 ml of tissue lysis buffer (50 mM Tris, 150 mM NaCl, 0.1% Ipegal, 10% glycerol). Protein content was determined

by BCA assay (Promega) and equal amounts of protein were loaded (30 mg/lane) after boiling for 5-min in 2X SDS sample buffer. All samples were run on 8–16% Tris-glycine gels. Unc45b antibody (Sigma) was used at a concentration of 1:500. IκB and NF-κB antibodies (Cell Signaling) were used at 1:1000. TDP-43 antibody (Proteintech) was used at 1:1200.

Immunohistochemistry and TEM

Paraffin-embedded brain and muscle sections were processed with antigen unmasking solution (Vector Labs) and stained using the Impress immunolabeling system as directed (Vector Labs). Anti-TDP-43 antibody was used at a concentration of 1:1000 and anti-ubiquitin antibody (Cell Signaling) was used at 1:2500. For immunofluorescence, frozen sections were permeabilized in PBS with 0.1% Triton X-100 followed by blocking in 5% normal goat serum. Sections were incubated in primary antibody overnight followed by staining with fluorescent secondary antibodies (Molecular Probes 1:500) for 1 h at room temperature. For TEM, mice were perfuse with 4% glutaraldehyde in 0.1 M cacodylate buffer and were post-fixed in 1% OsO4 and en bloc stained with 1% uranyl acetate. After standard dehydration, samples were infiltrated and embedded in Spurr low-viscosity resin (Electron Microscopy Sciences), and polymerized at 60°C for 18 h. Semi-thin sections (0.5 μm) were stained with toluidine blue, and 600–900 Å sections were stained in grids with Reynold's lead citrate and uranyl acetate.

Micro-CT analysis

Three animals from each genotype were anesthetized and sacrificed, and the left and right hind limbs were fixed in 4% PFA for 24 h following perfusion. Each entire femur was scanned using an eXplore Locus SP micro-CT scanner (GE Healthcare, Waukesha, WI, USA). The following scan parameters were used: tube voltage/current = 80 kVp/80 μA, beam filter = 250 μm thick aluminum, integration time = 1.7 s, detector binning = 2 × 2, views = 400, angular increment = 0.5°, signal averages = 8, scan time = 2 h. Image data were reconstructed at an isotropic resolution of 16 μm. Stereological analysis was performed using MicroView software (GE Healthcare) to generate a volumetric region of interest in the distal end of each femur in which trabecular bone was quantified. The following standard stereological parameters were computed as averages from values corresponding to the *x*, *y* and *z* axes: bone volume to total volume ratio (bone volume fraction), bone surface to bone volume ratio, trabecular thickness, trabecular spacing, trabecular number density (spatial frequency) and Euler number (measure of trabecular network connectivity). For qualitative comparisons in Figure 7, image data were displayed using OsiriX software (www.osirix-viewer.com). In Figure 7A, maximum intensity projection views of each distal femur were made by projecting through 500 μm-thick slabs in the reformatted coronal (top row) and sagittal (bottom row) planes. In Figure 7B, both 'red glass' translucent and solid color opaque volume rendering was used to show each distal femur under identical display settings.

Cell culture

C2C12 cells were maintained in Dulbecco's Modified Eagles Medium with 20% fetal bovine serum in 5% CO_2. Cells were grown to ~70% confluence and then transfected with Lipofectamine 2000 according to the manufacturer's directions. NF-κB and control luciferase reporter constructs were obtained from Clonetech (pMetLuc2-Reporter, pNF-κB-MetLuc2-Reporter) and activity was determined using the accompanying 'Ready to glow' secreted luciferase assay kit as directed. Luciferase activity was read using a Vector 5 plate reader.

SUPPLEMENTARY MATERIAL

Supplementary Material is available at *HMG* online.

ACKNOWLEDGEMENTS

We are indebted to Steve Greenberg for helpful discussion about IBM, and to David Dempster and David Roodman for helpful discussion about PDB. We also thank Gillian Ritson and Natalia Nedelsky for their support and critical reading and editing of the manuscript. We thank Mareike Schroff for her excellent technical assistance with the TDP-43 muscle pathology. We also thank Debra Horng for her assistance with the bone micro-CT analysis.

Conflict of Interest statement. None declared.

FUNDING

Funding for this work was provided by Deutsche Forschungsgemeinschaft (SFB 596) to M.N.; and from the Association of Frontotemporal Dementias, the Dana Foundation and the Packard Foundation for ALS Research at Johns Hopkins University, the Comprehensive Neuroscience Center at the University of Pennsylvania, and the American-Syrian-Lebanese Associated Charities to J.P.T.

REFERENCES

1. Kimonis, V.E., Kovach, M.J., Waggoner, B., Leal, S., Salam, A., Rimer, L., Davis, K., Khardori, R. and Gelber, D. (2000) Clinical and molecular studies in a unique family with autosomal dominant limb-girdle muscular dystrophy and Paget disease of bone. *Genet. Med.*, **2**, 232–241.
2. Forman, M.S., Mackenzie, I.R., Cairns, N.J., Swanson, E., Boyer, P.J., Drachman, D.A., Jhaveri, B.S., Karlawish, J.H., Pestronk, A., Smith, T.W. *et al.* (2006) Novel ubiquitin neuropathology in frontotemporal dementia with valosin-containing protein gene mutations. *J. Neuropathol. Exp. Neurol.*, **65**, 571–581.
3. Watts, G.D., Wymer, J., Kovach, M.J., Mehta, S.G., Mumm, S., Darvish, D., Pestronk, A., Whyte, M.P. and Kimonis, V.E. (2004) Inclusion body myopathy associated with Paget disease of bone and frontotemporal dementia is caused by mutant valosin-containing protein. *Nat. Genet.*, **36**, 377–381.
4. Haubenberger, D., Bittner, R.E., Rauch-Shorny, S., Zimprich, F., Mannhalter, C., Wagner, L., Mineva, I., Vass, K., Auff, E. and Zimprich, A. (2005) Inclusion body myopathy and Paget disease is linked to a novel mutation in the VCP gene. *Neurology*, **65**, 1304–1305.
5. Gidaro, T., Modoni, A., Sabatelli, M., Tasca, G., Broccolini, A. and Mirabella, M. (2008) An Italian family with inclusion-body myopathy and

frontotemporal dementia due to mutation in the VCP gene. *Muscle Nerve*, **37**, 111–114.
6. Bersano, A., Del Bo, R., Lamperti, C., Ghezzi, S., Fagiolari, G., Fortunato, F., Ballabio, E., Moggio, M., Candelise, L., Galimberti, D. *et al.* (2009) Inclusion body myopathy and frontotemporal dementia caused by a novel VCP mutation. *Neurobiol. Aging*, **30**, 752–758.
7. Viassolo, V., Previtali, S.C., Schiatti, E., Magnani, G., Minetti, C., Zara, F., Grasso, M., Dagna-Bricarelli, F. and Di Maria, E. (2008) Inclusion body myopathy, Paget's disease of the bone and frontotemporal dementia: recurrence of the VCP R155H mutation in an Italian family and implications for genetic counselling. *Clin. Genet.*, **74**, 54–60.
8. Djamshidian, A., Schaefer, J., Haubenberger, D., Stogmann, E., Zimprich, F., Auff, E. and Zimprich, A. (2009) A novel mutation in the VCP gene (G157R) in a German family with inclusion-body myopathy with Paget disease of bone and frontotemporal dementia. *Muscle Nerve*, **39**, 389–391.
9. Muller, J.M., Deinhardt, K., Rosewell, I., Warren, G. and Shima, D.T. (2007) Targeted deletion of p97 (VCP/CDC48) in mouse results in early embryonic lethality. *Biochem. Biophys. Res. Commun.*, **354**, 459–465.
10. Weihl, C.C., Pestronk, A. and Kimonis, V.E. (2009) Valosin-containing protein disease: inclusion body myopathy with Paget's disease of the bone and fronto-temporal dementia. *Neuromuscul. Disord.*, **19**, 308–315.
11. Kakizuka, A. (2008) Roles of VCP in human neurodegenerative disorders. *Biochem. Soc. Trans.*, **36**, 105–108.
12. Ju, J.S., Fuentealba, R.A., Miller, S.E., Jackson, E., Piwnica-Worms, D., Baloh, R.H. and Weihl, C.C. (2009) Valosin-containing protein (VCP) is required for autophagy and is disrupted in VCP disease. *J. Cell. Biol.*, **187**, 875–888.
13. Tresse, E., Salomons, F.A., Vesa, J., Bott, L.C., Kimonis, V., Yao, T.P., Dantuma, N.P. and Taylor, J.P. VCP/p97 is essential for maturation of ubiquitin-containing autophagosomes and this function is impaired by mutations that cause IBMPFD. *Autophagy*, **6**, 217–227.
14. Guinto, J.B., Ritson, G.P., Taylor, J.P. and Forman, M.S. (2007) Valosin-containing protein and the pathogenesis of frontotemporal dementia associated with inclusion body myopathy. *Acta. Neuropathol.*, **114**, 55–61.
15. Neumann, M., Sampathu, D.M., Kwong, L.K., Truax, A.C., Micsenyi, M.C., Chou, T.T., Bruce, J., Schuck, T., Grossman, M., Clark, C.M. *et al.* (2006) Ubiquitinated TDP-43 in frontotemporal lobar degeneration and amyotrophic lateral sclerosis. *Science*, **314**, 130–133.
16. Weihl, C.C., Miller, S.E., Hanson, P.I. and Pestronk, A. (2007) Transgenic expression of inclusion body myopathy associated mutant p97/VCP causes weakness and ubiquitinated protein inclusions in mice. *Hum. Mol. Genet.*, **16**, 919–928.
17. Kawai, M., Bessho, K., Kaihara, S., Sonobe, J., Oda, K., Iizuka, T. and Maruyama, H. (2003) Ectopic bone formation by human bone morphogenetic protein-2 gene transfer to skeletal muscle using transcutaneous electroporation. *Hum. Gene. Ther.*, **14**, 1547–1556.
18. Ueno, N., Inui, A., Iwamoto, M., Kaga, T., Asakawa, A., Okita, M., Fujimiya, M., Nakajima, Y., Ohmoto, Y., Ohnaka, M. *et al.* (1999) Decreased food intake and body weight in pancreatic polypeptide-overexpressing mice. *Gastroenterology*, **117**, 1427–1432.
19. Ray, P.S., Martin, J.L., Swanson, E.A., Otani, H., Dillmann, W.H. and Das, D.K. (2001) Transgene overexpression of alphaB crystallin confers simultaneous protection against cardiomyocyte apoptosis and necrosis during myocardial ischemia and reperfusion. *FASEB. J.*, **15**, 393–402.
20. Bruijn, L.I., Becher, M.W., Lee, M.K., Anderson, K.L., Jenkins, N.A., Copeland, N.G., Sisodia, S.S., Rothstein, J.D., Borchelt, D.R., Price, D.L. *et al.* (1997) ALS-linked SOD1 mutant G85R mediates damage to astrocytes and promotes rapidly progressive disease with SOD1-containing inclusions. *Neuron*, **18**, 327–338.
21. Reddy, P.H., Charles, V., Williams, M., Miller, G., Whetsell, W.O. Jr and Tagle, D.A. (1999) Transgenic mice expressing mutated full-length HD cDNA: a paradigm for locomotor changes and selective neuronal loss in Huntington's disease. *Philos. Trans. R. Soc. Lond. B. Biol. Sci.*, **354**, 1035–1045.
22. Kimonis, V.E., Mehta, S.G., Fulchiero, E.C., Thomasova, D., Pasquali, M., Boycott, K., Neilan, E.G., Kartashov, A., Forman, M.S., Tucker, S. *et al.* (2008) Clinical studies in familial VCP myopathy associated with Paget disease of bone and frontotemporal dementia. *Am. J. Med. Genet. A*, **146A**, 745–757.
23. Amato, A.A. and Barohn, R.J. (2009) Inclusion body myositis: old and new concepts. *J. Neurol. Neurosurg. Psychiatry*, **80**, 1186–1193.
24. Broccolini, A., Gidaro, T., Morosetti, R. and Mirabella, M. (2009) Hereditary inclusion-body myopathy: clues on pathogenesis and possible therapy. *Muscle Nerve*, **40**, 340–349.
25. Gitcho, M.A., Strider, J., Carter, D., Taylor-Reinwald, L., Forman, M.S., Goate, A.M. and Cairns, N.J. (2009) VCP mutations causing frontotemporal lobar degeneration disrupt localization of TDP-43 and induce cell death. *J. Biol. Chem.*, **284**, 12384–12398.
26. Weihl, C.C., Temiz, P., Miller, S.E., Watts, G., Smith, C., Forman, M., Hanson, P.I., Kimonis, V. and Pestronk, A. (2008) TDP-43 accumulation in inclusion body myopathy muscle suggests a common pathogenic mechanism with frontotemporal dementia. *J Neurol. Neurosurg. Psychiatry*, **79**, 1186–1189.
27. Kim, J., Lowe, T. and Hoppe, T. (2008) Protein quality control gets muscle into shape. *Trends. Cell. Biol.*, **18**, 264–272.
28. Wohlgemuth, S.L., Crawford, B.D. and Pilgrim, D.B. (2007) The myosin co-chaperone UNC-45 is required for skeletal and cardiac muscle function in zebrafish. *Dev. Biol.*, **303**, 483–492.
29. Janiesch, P.C., Kim, J., Mouysset, J., Barikbin, R., Lochmuller, H., Cassata, G., Krause, S. and Hoppe, T. (2007) The ubiquitin-selective chaperone CDC-48/p97 links myosin assembly to human myopathy. *Nat. Cell. Biol.*, **9**, 379–390.
30. Neumann, M., Mackenzie, I.R., Cairns, N.J., Boyer, P.J., Markesbery, W.R., Smith, C.D., Taylor, J.P., Kretzschmar, H.A., Kimonis, V.E. and Forman, M.S. (2007) TDP-43 in the ubiquitin pathology of frontotemporal dementia with VCP gene mutations. *J Neuropathol. Exp. Neurol.*, **66**, 152–157.
31. Davidson, Y., Kelley, T., Mackenzie, I.R., Pickering-Brown, S., Du Plessis, D., Neary, D., Snowden, J.S. and Mann, D.M. (2007) Ubiquitinated pathological lesions in frontotemporal lobar degeneration contain the TAR DNA-binding protein, TDP-43. *Acta. Neuropathol.*, **113**, 521–533.
32. Lalonde, R., Kim, H.D., Maxwell, J.A. and Fukuchi, K. (2005) Exploratory activity and spatial learning in 12-month-old APP(695)SWE/co+PS1/DeltaE9 mice with amyloid plaques. *Neurosci. Lett.*, **390**, 87–92.
33. Allen, B., Ingram, E., Takao, M., Smith, M.J., Jakes, R., Virdee, K., Yoshida, H., Holzer, M., Craxton, M., Emson, P.C. *et al.* (2002) Abundant tau filaments and nonapoptotic neurodegeneration in transgenic mice expressing human P301S tau protein. *J. Neurosci.*, **22**, 9340–9351.
34. Tarantino, L.M., Gould, T.J., Druhan, J.P. and Bucan, M. (2000) Behavior and mutagenesis screens: the importance of baseline analysis of inbred strains. *Mamm. Genome*, **11**, 555–564.
35. Geser, F., Brandmeir, N.J., Kwong, L.K., Martinez-Lage, M., Elman, L., McCluskey, L., Xie, S.X., Lee, V.M. and Trojanowski, J.Q. (2008) Evidence of multisystem disorder in whole-brain map of pathological TDP-43 in amyotrophic lateral sclerosis. *Arch. Neurol.*, **65**, 636–641.
36. Ittner, L.M., Fath, T., Ke, Y.D., Bi, M., van Eersel, J., Li, K.M., Gunning, P. and Gotz, J. (2008) Parkinsonism and impaired axonal transport in a mouse model of frontotemporal dementia. *Proc. Natl. Acad. Sci. USA*, **105**, 15997–16002.
37. Sennvik, K., Boekhoorn, K., Lasrado, R., Terwel, D., Verhaeghe, S., Korr, H., Schmitz, C., Tomiyama, T., Mori, H., Krugers, H. *et al.* (2007) Tau-4R suppresses proliferation and promotes neuronal differentiation in the hippocampus of tau knockin/knockout mice. *FASEB. J.*, **21**, 2149–2161.
38. Crawley, J.N., Belknap, J.K., Collins, A., Crabbe, J.C., Frankel, W., Henderson, N., Hitzemann, R.J., Maxson, S.C., Miner, L.L., Silva, A.J. *et al.* (1997) Behavioral phenotypes of inbred mouse strains: implications and recommendations for molecular studies. *Psychopharmacology (Berl)*, **132**, 107–124.
39. Lucas, G.J., Daroszewska, A. and Ralston, S.H. (2006) Contribution of genetic factors to the pathogenesis of Paget's disease of bone and related disorders. *J. Bone. Miner. Res.*, **21** (Suppl. 2), P31–P37.
40. Halawani, D. and Latterich, M. (2006) p97: The cell's molecular purgatory? *Mol. Cell.*, **22**, 713–717.
41. Dai, R.M., Chen, E., Longo, D.L., Gorbea, C.M. and Li, C.C. (1998) Involvement of valosin-containing protein, an ATPase Co-purified with IkappaBalpha and 26 S proteasome, in ubiquitin-proteasome-mediated degradation of IkappaBalpha. *J. Biol. Chem.*, **273**, 3562–3573.
42. Asai, T., Tomita, Y., Nakatsuka, S., Hoshida, Y., Myoui, A., Yoshikawa, H. and Aozasa, K. (2002) VCP (p97) regulates NFkappaB signaling pathway, which is important for metastasis of osteosarcoma cell line. *Jpn. J. Cancer Res.*, **93**, 296–304.

43. Vandermoere, F., El Yazidi-Belkoura, I., Slomianny, C., Demont, Y., Bidaux, G., Adriaenssens, E., Lemoine, J. and Hondermarck, H. (2006) The valosin-containing protein (VCP) is a target of Akt signaling required for cell survival. *J. Biol. Chem.*, **281**, 14307–14313.
44. Soysa, N.S. and Alles, N. (2009) NF-kappaB functions in osteoclasts. *Biochem. Biophys. Res. Commun.*, **378**, 1–5.
45. Hiruma, Y., Kurihara, N., Subler, M.A., Zhou, H., Boykin, C.S., Zhang, H., Ishizuka, S., Dempster, D.W., Roodman, G.D. and Windle, J.J. (2008) A SQSTM1/p62 mutation linked to Paget's disease increases the osteoclastogenic potential of the bone microenvironment. *Hum. Mol. Genet.*, **17**, 3708–3719.
46. Najat, D., Garner, T., Hagen, T., Shaw, B., Sheppard, P.W., Falchetti, A., Marini, F., Brandi, M.L., Long, J.E., Cavey, J.R. *et al.* (2009) Characterization of a non-UBA domain missense mutation of sequestosome 1 (SQSTM1) in Paget's disease of bone. *J. Bone Miner. Res.*, **24**, 632–642.
47. Rea, S.L., Walsh, J.P., Ward, L., Magno, A.L., Ward, B.K., Shaw, B., Layfield, R., Kent, G.N., Xu, J. and Ratajczak, T. (2009) Sequestosome 1 mutations in Paget's disease of bone in Australia: prevalence, genotype/phenotype correlation, and a novel non-UBA domain mutation (P364S) associated with increased NF-kappaB signaling without loss of ubiquitin binding. *J. Bone Miner. Res.*, **24**, 1216–1223.
48. Chamoux, E., Couture, J., Bisson, M., Morissette, J., Brown, J.P. and Roux, S. (2009) The p62 P392L mutation linked to Paget's disease induces activation of human osteoclasts. *Mol. Endocrinol.*, **23**, 1668–1680.
49. Peterson, J.M. and Guttridge, D.C. (2008) Skeletal muscle diseases, inflammation, and NF-kappaB signaling: insights and opportunities for therapeutic intervention. *Int. Rev. Immunol.*, **27**, 375–387.
50. Cai, D., Frantz, J.D., Tawa, N.E. Jr, Melendez, P.A., Oh, B.C., Lidov, H.G., Hasselgren, P.O., Frontera, W.R., Lee, J., Glass, D.J. *et al.* (2004) IKKbeta/NF-kappaB activation causes severe muscle wasting in mice. *Cell*, **119**, 285–298.
51. Salajegheh, M., Pinkus, J.L., Taylor, J.P., Amato, A.A., Nazareno, R., Baloh, R.H. and Greenberg, S.A. (2009) Sarcoplasmic redistribution of nuclear TDP-43 in inclusion body myositis. *Muscle Nerve*, **40**, 19–31.
52. Kusters, B., van Hoeve, B.J., Schelhaas, H.J., Ter Laak, H., van Engelen, B.G. and Lammens, M. (2009) TDP-43 accumulation is common in myopathies with rimmed vacuoles. *Acta. Neuropathol.*, **117**, 209–211.
53. DeLaBarre, B. and Brunger, A.T. (2005) Nucleotide dependent motion and mechanism of action of p97/VCP. *J. Mol. Biol.*, **347**, 437–452.
54. Halawani, D., LeBlanc, A.C., Rouiller, I., Michnick, S.W., Servant, M.J. and Latterich, M. (2009) Hereditary inclusion body myopathy-linked p97/VCP mutations in the NH2 domain and the D1 ring modulate p97/VCP ATPase activity and D2 ring conformation. *Mol. Cell. Biol.*, **29**, 4484–4494.
55. Wu, C. and Ghosh, S. (1999) beta-TrCP mediates the signal-induced ubiquitination of IkappaBbeta. *J. Biol. Chem.*, **274**, 29591–29594.
56. Suzuki, H., Chiba, T., Kobayashi, M., Takeuchi, M., Suzuki, T., Ichiyama, A., Ikenoue, T., Omata, M., Furuichi, K. and Tanaka, K. (1999) IkappaBalpha ubiquitination is catalyzed by an SCF-like complex containing Skp1, cullin-1, and two F-box/WD40-repeat proteins, betaTrCP1 and betaTrCP2. *Biochem. Biophys. Res. Commun.*, **256**, 127–132.